

MIT Open Access Articles

Modelling and simulation of in-orbit centrifugal casting of a paraffin wax grain inside a 3U CubeSat

The MIT Faculty has made this article openly available. **Please share** how this access benefits you. Your story matters.

Citation: Leuteri Costanzo, Daniele, Stober, Keith Javier, Wood, Danielle and Colombo, Camilla. 2021. "Modelling and simulation of in-orbit centrifugal casting of a paraffin wax grain inside a 3U CubeSat." AIAA Propulsion and Energy 2021 Forum.

As Published: 10.2514/6.2021-3503

Publisher: American Institute of Aeronautics and Astronautics (AIAA)

Persistent URL: <https://hdl.handle.net/1721.1/146531>

Version: Author's final manuscript: final author's manuscript post peer review, without publisher's formatting or copy editing

Terms of use: Creative Commons Attribution-Noncommercial-Share Alike



Modelling and Simulation of In-Orbit Centrifugal Casting of a Paraffin Wax Grain Inside a 3U CubeSat

Daniele Leuteri Costanzo*, Keith Javier Stober†, Danielle Wood‡, and Camilla Colombo§
Politecnico di Milano, Milan, Italy, 20158
Massachusetts Institute of Technology, Cambridge, MA, 02139

The purpose of this research is to explore the possibility of using paraffin wax as fuel to deorbit small satellites, potential mean to tackle space debris mitigation. Experiments conducted by the Space Enabled Research Group have been characterised by the use of paraffin as working fluid, with rotation rates ranging from 50-1500 rpm, and initial temperature of 75-100 °C. The work conducted by the authors investigates the possibility of performing centrifugal casting of paraffin into annular shapes while the spacecraft is in orbit. The adopted strategy considers using the wax as thermal insulator and, at the end-of-life, recast it as fuel to allow a controlled reentry of the satellite. The workflow is conceived such that the wax will be melted and conveyed into the combustion chamber, which - spun by a DC motor - allows the wax to be shaped into a hollow cylinder. This paper describes the results obtained from a parametric system-level simulation tool, developed in a Matlab/Simulink environment, for the simulation of the thermal behavior of a spacecraft in Earth orbit, as well as performing mission analysis and thermal control design.

I. Nomenclature

A	=	area
a	=	albedo coefficient
α	=	absorptivity coefficient
d	=	disturbance torque
ΔV	=	delta velocity
ϵ	=	emissivity coefficient
F	=	view factor
\mathbf{F}	=	force
g_0	=	standard sea-level gravity acceleration
I_x, I_y, I_z	=	moments of inertia of the spacecraft
I_r	=	moment of inertia of the internal rotating device
I_{sp}	=	specific impulse
\dot{m}	=	mass flow rate
μ	=	Earth's gravitational constant
\mathbf{p}	=	orbital perturbation
Q	=	heat flux
r	=	radius
\mathbf{r}	=	position vector in cartesian coordinates
$\dot{\mathbf{r}}$	=	velocity vector in cartesian coordinates
$\ddot{\mathbf{r}}$	=	acceleration vector in cartesian coordinates
S	=	heat flux per unit area
T	=	temperature
\mathbf{T}	=	thrust vector
t_b	=	burning time

*Space Systems Engineer, D-Orbit, Fino Mornasco, Italy, 22073

†Research Engineer, Space Enabled Research Group, MIT Media Lab, AIAA Member

‡Assistant Professor; Director, Space Enabled Research Group, MIT Media Lab

§Associate Professor; Politecnico di Milano, Department of Aerospace Science and Technology

TOF = time of flight
 u = control torque
 ω = angular velocity
 $\dot{\omega}$ = angular acceleration
 rpm = revolutions per minute

II. Introduction

THE extreme environment at which a spacecraft is exposed during its lifetime makes it unthinkable not to design a thermal control system, as the excessive temperature gradients and heat loads will generate permanent damages and changes in the physical, thermal and optical properties of the spacecraft and its components.

Since the idea behind this project is to use, in the first stage, the paraffin as thermal insulator, the reader will find in the current section a brief literature review on existing projects exploiting paraffin for this specific use case. More details about the whole experiment will be unveiled later on.

The main classification for the thermal control is that it can be either active or passive. NASA, with its IceCube mission, exploited the use of paraffin wax in the form of Phase Change Material (PCM) packs to insulate some components, in order to meet the requirements in terms of operating temperature ranges [1].

In this framework, the paraffin is cast into small packs and they are attached near the components of interest, as in Figure 1; whereas, a detail of these 3 packs can be appreciated in Figure 2.

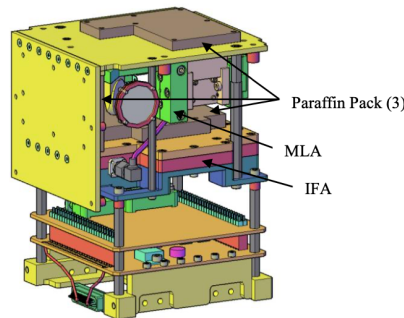


Fig. 1 Configuration with 3 mini-paraffin packs for the IceCube spacecraft [1]

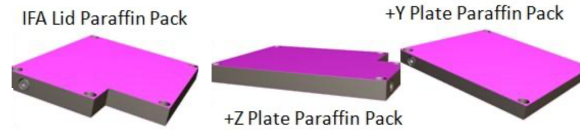


Fig. 2 Detail of the three mini-paraffin packs [1]

Therefore, the adopted strategy is to use the paraffin to accumulate heat when the two components are switched on and to dissipate it, through radiators, when they are switched off. During these operations, the phase of the paraffin varies, going from solid to liquid state (thus, the name *phase change materials*).

This project is more ambitious, in the sense that the wax is meant to be used as propellant at the end of life, therefore a system capable of conveying the melted paraffin inside the combustion chamber shall be adopted.

The purpose of this project, which gave birth to the collaboration between Massachusetts Institute of Technology's Space Enabled [2] and Politecnico di Milano, within the COMPASS ERC project [3], is to explore the possibility of using wax as a fuel for small satellites. The main reason is to overcome the toxicity of the most conventional and currently adopted propellants, such as hydrazine and nitrogen tetroxide. Candle wax seems to be suitable for the job.

The investigation is about the possibility to perform centrifugal casting of paraffin into annular shapes both on Earth and in microgravity. The aim of this project is to use, at the Beginning Of Life (BOL) the wax as a thermal insulator and,

at the End Of Life (EOL), recast it as a fuel to allow a controlled re-entry. The expectations are that the microgravity environment will reduce the rotation rates required to cast the wax into the desired shape.

The currently conducted experiments at 1 g conditions have been characterized by the use of paraffin wax and beeswax as working fluids, with rotation rates ranging from 50-1500 rpm, and an initial temperature of 75-100 °C. The idea, then, is to melt the wax originally used as thermal insulator, with the purpose of using it as a thermal insulator, and convey it into the combustion chamber, which will spin at a certain rate, allowing the wax to be shaped into a caved cylinder, which is one of the most efficient shapes to burn the wax. For more details on the vision of Space Enabled research group, the interested reader can find more details in [2].

This work is developed under one main assumption: the wax is already inside the combustion chamber, and the simulations conducted will take into account the grain formation mode and what comes after it (i.e. maintaining the temperature below the melting one, perform the required attitude maneuvers for Earth pointing and, then, design de re-entry trajectory).

The aim of this work is to develop a parametric tool, with working environment set to be Matlab/Simulink, for the simulation of the thermal behavior of a spacecraft in Earth orbit, as well as performing mission analysis and thermal control design.

Such tool shall be able to couple the orbital dynamics with the Attitude Determination and Control System (ADCS), and both with the thermal environment, in order to obtain the temperature profile of the paraffin wax unit and see how it behaves under the effect of the external environmental fluxes.

It is important to remark that while this work involves the implementation of all the aforementioned phases, it is assumed - for the thermal analysis - that the liquefied wax is already being transported inside the combustion chamber. Therefore, the design of the thermal bus that shall convey it from its initial form as PCM into the cylinder will not be part of this work. The simulation will take place, then, by considering the liquid wax just injected inside the combustion chamber, its rotation (in order to allow the formation of the grain) which lasts around 45 minutes, and then the focus will be mainly on the thermal control, in order to keep it below 75 °C.

All the data relative to the paraffin wax has been derived experimentally by the Space Enabled research group, and the polymer considered in this work has the formula of $C_{32}H_{66}$.

III. Grain Formation Mode

Among all of the mission modes, this is - for sure - the most important and peculiar one. Technically, this phase is composed of two parts: the first one is devoted in melting the wax and conveying it into the combustion chamber, the second is the one where the liquid wax is inside the cylinder and then - by means of an external DC brushed motor - it starts rotating in order to exploit centrifugal forces for distributing the paraffin over the walls; once finished the process, it solidifies and the grain is ready to be used for the deorbit of the spacecraft.

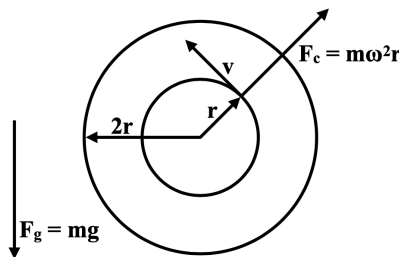


Fig. 3 Schematic representation of the problem [4]

At this point, the first part has not been engineered yet, and so this work assumes that the wax is already inside the combustion chamber and only the event related to the rotation is considered, in order to check - mainly that the stability of the spacecraft is preserved.

From previous investigations [4], the adopted setup is the one in Figure 4

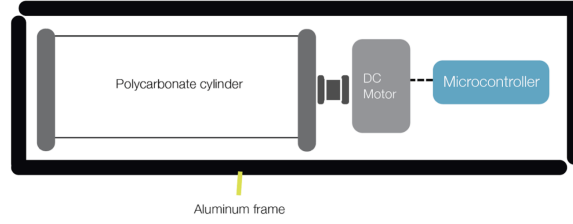


Fig. 4 Laboratory experiment setup [4]

The configuration has already been described, and taking into account the brushless motor, the whole apparatus is expected to occupy up to 1.5 U.

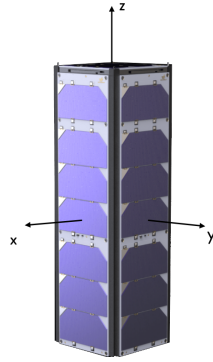


Fig. 5 Spacecraft body-fixed reference frame

In order to take this effect into account for the attitude stability, the overall spacecraft plus the internal rotational device has been modeled according to a dual spin spacecraft configuration; therefore, since the rotation acts along the z-axis (directed as in 5, the dynamics of the spacecraft can be represented as:

$$\begin{cases} \dot{\omega}_x = \frac{I_y - I_z}{I_x} \omega_y \omega_z - \frac{I_r \omega_r \omega_y}{I_x} + \frac{d_x}{I_x} + \frac{u_x}{I_x} \\ \dot{\omega}_y = \frac{I_z - I_x}{I_y} \omega_x \omega_z + \frac{I_r \omega_r \omega_x}{I_y} + \frac{d_y}{I_y} + \frac{u_y}{I_y} \\ \dot{\omega}_z = \frac{I_x - I_y}{I_z} \omega_x \omega_y - I_r \omega_r + \frac{d_z}{I_z} + \frac{u_z}{I_z} \end{cases} \quad (1)$$

where I_x, I_y and I_z are the moments of inertia of the whole spacecraft, $\omega_x, \omega_y, \omega_z$ are the spacecraft's angular velocities expressed in the body frame, I_r and ω_r are the ones of the cylinder, while d_i and u_i are the disturbance and control torques, respectively.

By simple mass geometry equations, the inertia of the cylinder can be computed as:

$$I_r = \frac{M_r}{2} (r_i^2 + r_e^2) \quad (2)$$

giving a moment of inertia of $2.3 \cdot 10^{-3} \text{ kg} \cdot \text{m}^2$, i.e. one order of magnitude smaller than the inertia moment of the spacecraft about the z-axis; this should hint that the attitude won't be strongly affected, given also the fact that - once it will spin at its maximum rate, which is expected to be 500 rpm, it should increase the gyroscopic stiffness.

To account for the DC motor, the input signal used to model its behavior is the one in Figure 6, i.e. a fade-in fade-out signal, with symmetric windows for its rise and decay of about 300 ms.

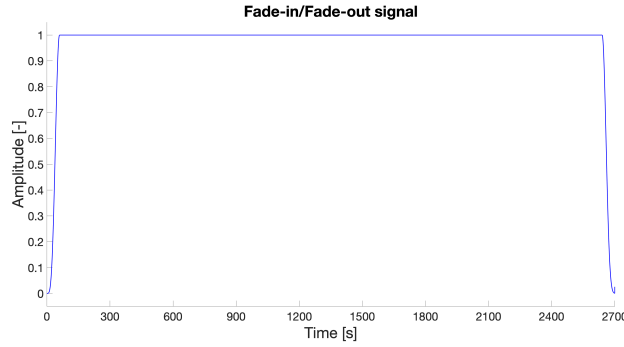


Fig. 6 Input signal - Grain formation

After that the unitary amplitude input signal is generated, it is - then - amplified by means of a gain block, in order to take into account the actual amplitude of the maximum rotational rate, plus a Gaussian white noise so to account for non-modeled disturbances that will for sure arise in the real situation (e.g. sloshing effects).

The results are quite good, in terms of stability, and show that it is feasible - from the attitude point of view - to perform this operation. From Figure 7, the angular velocities show the effects of this spinning device, corresponding to the beginning and the ending of this phase. In particular, at the beginning, for a moment, the angular velocity along z drifts away from the equilibrium condition, but then - thanks to the optimal quaternion-based controller - it is quickly recovered and the stability, for the whole duration of the phase (which is assumed to last for about 45 minutes), is granted. After the device stops spinning, a peak is shown in the same plot, and this is due to the fact that the momentum is exchanged back between the device itself and the spacecraft. However, again the controller - whose torques are shown in Figure 9, intervenes and re-establishes the stability.

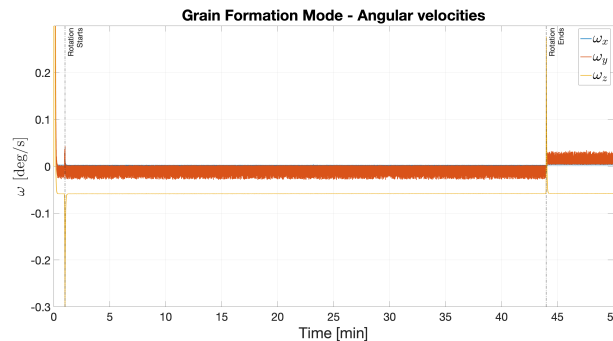


Fig. 7 Angular velocities - Grain formation

It was interesting to check also the pointing accuracy behavior during this phase. From Figure 8, it is possible to notice that this operation affects the pointing stability, indeed - even though it stays below 1° , it is still not suitable for picture acquisition; therefore, it should be better not to program picture acquisition while this mode is on.

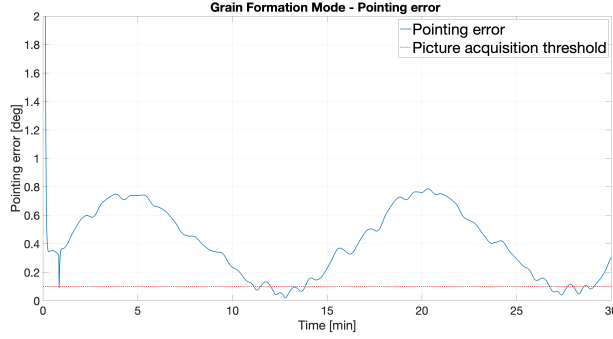


Fig. 8 Pointing error - Grain formation

In figure Figure 9 it is shown that the most stressed reaction wheel is the one acting along z. After this phase, a desaturation may be required. However, since the grain formation happens only at the end of life, there is no need to perform a momentum unloading, as the spacecraft will be injected into a graveyard orbit right away; this aspect will be further explained in the section concerning the deorbit trajectory design and optimisation.

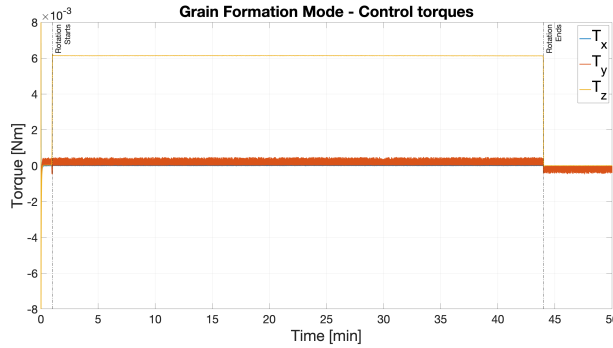


Fig. 9 Pointing error - Grain formation

Hence, from the attitude point of view, these simulations confirm that the stability of the spacecraft won't be affected, as hinted already by the first "guess" considerations derived from comparing the inertia of the cylinder and the one of the spacecraft.

IV. Thermal Environment Modelling

The thermal environment is what defines the boundary conditions at which the spacecraft is exposed. These are mainly determined by the orbital parameters, by the position of the Earth on the ecliptic, by external radiation sources (direct sunlight, Earth's albedo and infrared (IR) radiation).

Next, there will be a description of how these effects have been modeled and coupled with the orbital parameters and with the attitude.

A. Direct solar radiation

The first contribution taken into account is the radiation directly coming from the Sun. Such radiation is a function of the solar constant, $S_0 = 1322 \text{ W/m}^2$, which is basically the intensity of sunlight radiation, emitted at 1 AU (mean distance between Earth and Sun) and perpendicular to Earth's surface. Due to the fact that Earth's orbit around the sun is slightly elliptical, such value is not constant throughout the year; indeed, it ranges between $S_0 = 1322 \text{ W/m}^2$ at aphelion, to a maximum value of $S_0 = 1414 \text{ W/m}^2$ at perihelion, with a variation of $\pm 3.4\% \text{ W/m}^2$

To model this effect and take into account the heat fluxes balance, one might model the incoming solar flux as:

$$Q_{s,i} = \alpha_i A_i \cos(b_i) S_0 \quad (3)$$

where

$$\cos(b_i) = \mathbf{n}_i \cdot \mathbf{s} \quad (4)$$

where \mathbf{n}_i is the unit vector normal to the i -th surface of the satellite and \mathbf{s} is the solar vector.

To proceed down this road, both vectors \mathbf{n}_i and \mathbf{s} must be expressed in the same frame of reference. In order to couple this analysis not only with the orbital position, it has been decided to express both vectors in the body fixed reference frame.

In this way, the attitude, the orbit and the thermal environment are coupled with a high degree of accuracy.

Moreover, as already done with the solar radiation pressure model, also in this case the coupling affects this heat contribution: using the same shadow function, whenever the spacecraft is in Earth's shadow, $Q_s = 0 \text{ W/m}^2$, otherwise, it is computed as in Equation 3.

B. Reflected solar radiation

The solar radiation that hits the surface of the Earth and gets reflected is known as *albedo*. As we'll see with the infrared radiation, albedo varies across the globe, so depending on where we are located there will be a different value of reflected fraction of the incident solar flux. Therefore, in order to correctly account for it, one might adopt a model that takes into account the fact that the albedo coefficient, a , varies with latitude, longitude and time.

However, for sake of ease, it is assumed that the albedo coefficient is uniform around the globe; an averaged value is found to be $a = 0.273$ [5].

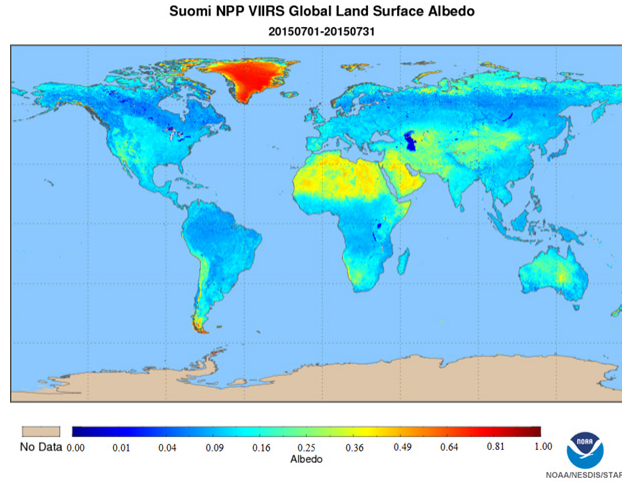


Fig. 10 Percentage of reflected solar flux, [6]

So, after dividing the surface of the Earth into patches (assumed to diffusely reflect equally in all the directions the incident radiation), it is possible to evaluate the infinitesimal contribution of a surface element, dS , as:

$$dQ_{A,i} = \alpha_i A_i a S_0 \frac{\cos(a_E) \cos(a_i) \cos(b_E)}{\pi \rho^2} dS \quad (5)$$

and, integrating over the whole surface:

$$Q_{A,i} = \alpha_i A_i a S_0 F_{A,i} \quad (6)$$

where $F_{A,i}$ is the albedo view factor of the i -th surface of the spacecraft, evaluated as:

$$F_{A,i} = \int_S \frac{\cos(a_E)\cos(a_i)\cos(b_E)}{\pi\rho^2} dS \quad (7)$$

In order to correctly evaluate this integral, all the vectors must be expressed in the same basis, and it is convenient to adopt a polar coordinate system.

This evaluation has been simplified, as the computational effort to evaluate the view factors while integrating the orbit equation was not compliant with the capabilities of the machine used to run such simulation. Therefore, it is assumed that the view factors are the same as the ones evaluated for the infrared radiation. But, in this case, the dependence on the spacecraft position shall be considered, just like it has been done for the direct solar flux. So, the albedo heat has been included in the model and expressed as a function of the position of the spacecraft, similarly to what has been done with the solar radiation. Of course, also in this case, when the spacecraft is in Earth's shadow, this contribution goes to zero, as no light is reflected by the portion of Earth at which the satellite is exposed.

C. Infrared radiation

Both albedo and IR heat loads depend on radiation wavelength and other factors that bring uncertainties in the model (such as weather conditions).

If Earth is divided into a series of patches, each can be seen as a diffuse radiator, with radiosity I_E , defined as the flux leaving the patch per unit area. Such value isn't constant, indeed it depends on where the patch is located, meaning that there are regions on Earth with higher values for IR emission, and regions where this contribution is lower. Just like the albedo, so, we could write $I_E = I_E(\lambda, \phi, t)$, with λ and ϕ being the longitude and latitude, describing in a polar coordinate system the position of a point on Earth's surface. However, for sake of ease, the value of I_E is assumed to be constant; a widely adopted value for a time-averaged infrared heat flux is $I_E = 213 \text{ W/m}^2$, and this is the value that will be used throughout this work.

Therefore, by neglecting the dependence on the satellite position, it is possible to write the infinitesimal contribution to the heat flux, $dQ_{E,i}$ by considering the emission of an infinitesimal surface element of the globe, dS , as:

$$dQ_{E,i} = \epsilon_i A_i I_E \frac{\cos(a_E)\cos(a_i)}{\pi\rho^2} dS \quad (8)$$

where:

- a_E is the angle between the normal to the patch element and the position vector of the spacecraft
- a_i is the angle between the position vector and the i -th normal of the surfaces of the spacecraft
- A_i and ϵ_i are the area and the emissivity of the i -th surface of the spacecraft
- ρ is the norm of the position vector of the spacecraft

integrating over all the surface elements:

$$Q_{E,i} = \epsilon_i A_i I_E F_{E,i} \quad (9)$$

where we find that:

$$F_{E,i} = \int_S \frac{\cos(a_E)\cos(a_i)}{\pi\rho^2} dS \quad (10)$$

is the radiative view factor, that can be evaluated by knowing the angles a_E and a_i , defined above.

In order to be correctly evaluated, this integral shall have all the terms written in the same reference frame, which has been chosen - again - to be the body fixed one; moreover, it can be convenient to write it in terms of appropriate polar coordinates.

Considering the attitude of the spacecraft described earlier, it can be shown that the view factor of the face $-x$ yields:

$$F_{E,-x} = \frac{1}{h^2} \quad (11)$$

	Internal Power, W	Solar flux, W/m^2	Albedo	Earth IR, W/m^2
Max	5	1414	0.35	270
Min	5	1322	0.273	220

Table 1 Heat fluxes for worst cold and hot case

whereas, for all the other surfaces:

$$F_{E,i} = -\frac{\sqrt{h^2 - 1}}{\pi h^2} + \frac{1}{\pi} \arctan\left(\frac{1}{\sqrt{h^2 - 1}}\right) \quad (12)$$

The only face that has null view factor is the one in the $+x$ direction, as it never faces Earth (in this particular locked attitude condition).

V. Thermal control design

The thermal control system must ensure that the spacecraft components operate within their allowable temperature ranges, in particular during the worst conditions. Such conditions are derived by considering the worst hot and cold cases, which - in this study - are given by the sunlight and eclipse.

For such purpose, a transient thermal analysis, rather than a steady-state one, has been performed, in order to fully account for the orbital and attitude dynamics; ideally, given the starting Julian day, the position of the spacecraft is computed at each time step with respect to the position of the sun, switching the thermal and albedo fluxes for each position of the spacecraft orbiting the Earth and, incidentally, the Sun.

The main character of this thermal analysis is, for sure, the paraffin wax. As already mentioned, in this work it is assumed that the wax is already inside the combustion chamber, and so the thermal analysis is focused only in trying to keep the grain below its melting temperature.

A. In-orbit thermal environment

The environmental values for the incoming heat fluxes are described in Table 1, while the internal generated power is assumed to be $5W$, due mainly to on-board electronic components.

Considering the equations described earlier for the computation of the heat fluxes, a nominal condition yields the loads in Figure 11

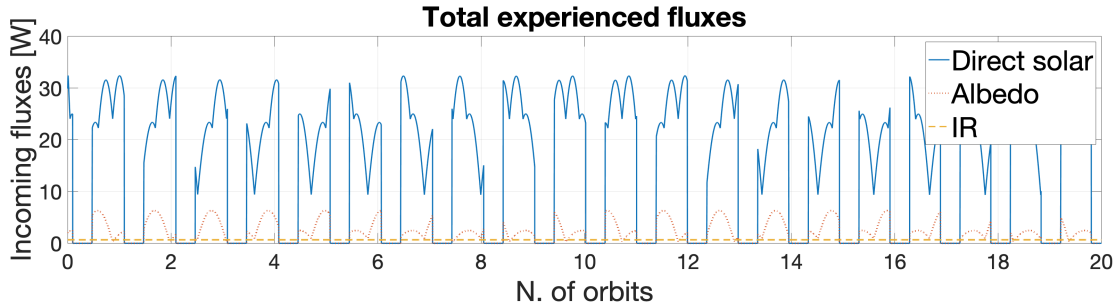


Fig. 11 Solar, albedo and IR fluxes

B. Passive thermal control design

In this stage of the mission, active thermal control methods are not needed; however, in the first part of the experiment, i.e. when the wax has to be melted, heaters might be sized, according to the strategy that the designer wants to adopt.

Assuming the structure of the spacecraft to be made of Aluminum 6061-T6, with body-mounted solar arrays, the optical properties are summarised in table 2

Material	Emissivity, ϵ	Absorbivity, α	Density, kg/m^3	Thermal conductivity, W/mK	Heat capacity, J/kgK
Solar cells	0.85	0.90	5307	20	325
Aluminum 6061-T6	0.055	0.38	2700	201	900

Table 2 Spacecraft external optical properties

For sake of ease, these properties can be averaged over the full effective area of the spacecraft, following the guidelines from [7] and [8] in this way:

$$\alpha_{ave} = f_c \alpha_{eff} + (1 - f_c) \alpha_u \quad (13)$$

where

- $f_c = 60.36\%$, as the area of a single cell is 30.18 cm^2 [9], and f_c represents the fraction of the face's area covered by solar cells (fig. 12)
- $\alpha_{eff} = \alpha_c - \eta$ is the effective cell absorbivity, function of the solar cells absorbivity, normally $\alpha_c = 0.91$ and of their efficiency; in this case, quad-junctions solar cells are considered [9], whose efficiency $\eta = 0.32$
- $\alpha_u = 0.5$ is the absorbivity of the surface non covered by solar cells yielding $\alpha_{ave} = 0.554$.

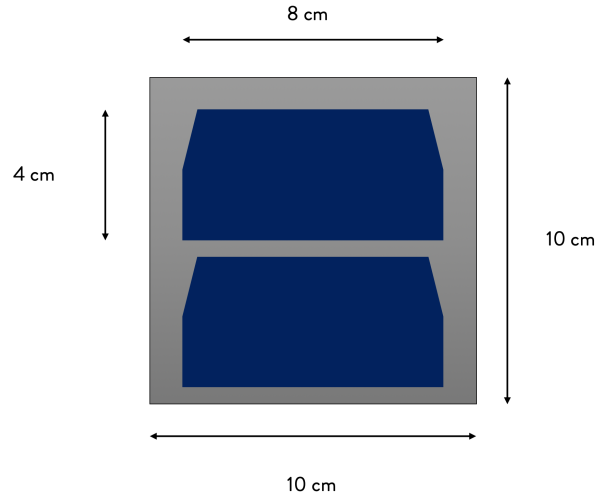


Fig. 12 Solar-cells covered face

The same can be done for the emissivity. Assuming $\epsilon_u = 0.05$, corresponding to a shiny metallic surface finish [5] for all the surfaces non covered by solar cells, an average value for the emissivity can be computed as:

$$\epsilon_{ave} = f_c \epsilon_c + (1 - f_c) \epsilon_u \quad (14)$$

where $\epsilon_c = 0.89$ [9], and so $\epsilon_{ave} = 0.557$.

C. Paraffin wax temperature constraints

The temperature ranges are set between 0 – 70°C; however, since the glass transition temperature of the paraffin wax is extremely low, the focus will be only into keeping it below 70°C.

D. Thermal control of the paraffin wax engine

To have an idea of what could be a suitable surface finish for the insulation of the wax engine, a parametric analysis involving the optical properties of the materials, in terms of absorptivity and emissivity, has been performed.

In this way, for a given temperature range, a set of values for α and ϵ have been evaluated. The temperature interval has been limited from 0 °C to 70 °C, as this is the range at which the paraffin wax can ideally work without melting.

Then, depending on the chosen orbital scenario, the tool will give back the plot in Figure 14

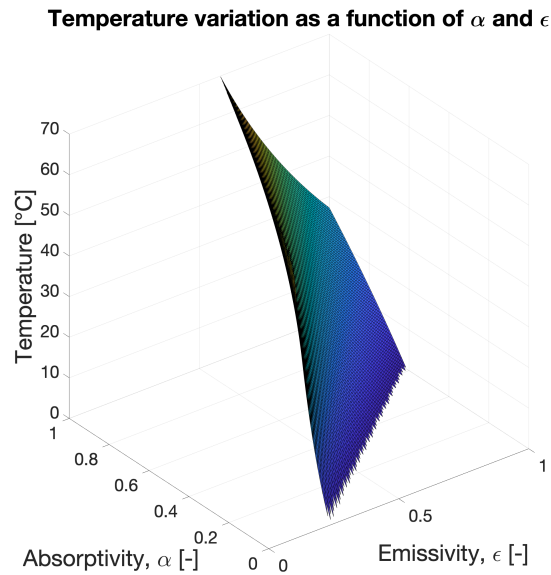


Fig. 13 Optical properties that grant the temperature to stay within the specified limits of 0 - 70 °C

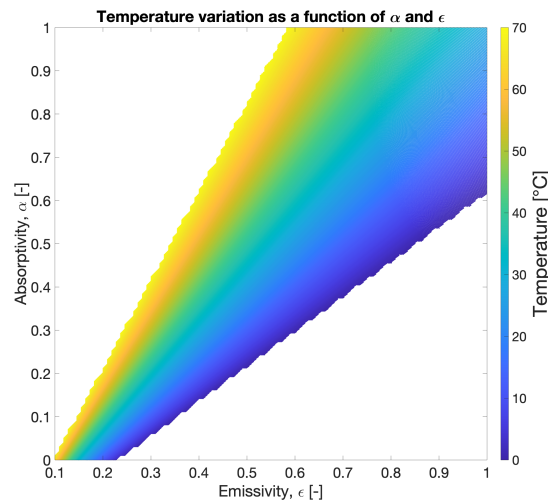


Fig. 14 Optical properties that grant the temperature to stay within the specified limits of 0 - 70 °C

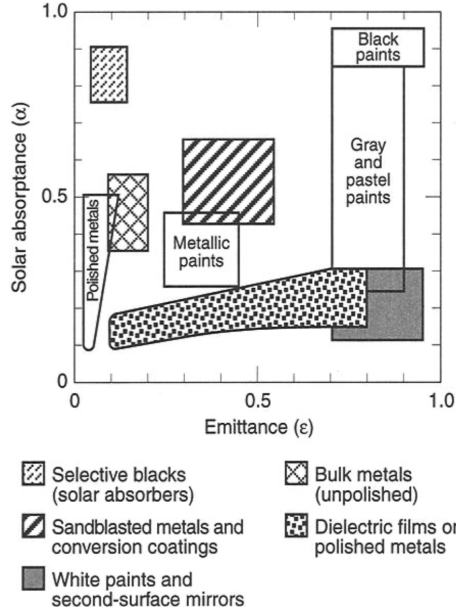


Fig. 15 Surface properties by type of finish, [5]

The parametric analysis hints the values of the optical properties that a material should have in order to keep it at temperatures near 60°C , and this turns out to be pretty useful and precise, in terms of results, as it will be shown in a while. Then, by overlapping figure 14 with 15 [5], a sandblasted metal cover for the engine can be used.

E. Multi-node model design on Matlab/Simulink

The mathematical formulation for the energy equation in vacuum conditions (i.e. in space) can neglect the convective heat transfer, and may be represented as:

$$\rho C_p \frac{\partial T}{\partial t} = \nabla \cdot q_c'' - \nabla \cdot q_r'' + q''' \quad (15)$$

where ρ is the density, C_p is the specific heat, T is the temperature. The first term on the right hand side of the equation, $\nabla \cdot q_c''$ is the energy addition per unit volume by conduction, $\nabla \cdot q_r''$ is the one due to radiation and the last term is the source term that accounts for internal heat dissipation (e.g. electronics, etc.).

At this point, based on the definition of conductive and radiative heat transfer given in the previous sections, based on a Thermal Network Approach, the final form of the energy equation can be represented as:

$$\frac{dT_i}{dt} \approx \frac{1}{(mC_p)_i} \left[\sum_{j=1}^N C_{i,j} (T_i - T_j) + \sum_{j=1}^N R_{i,j} (T_j^4 - T_i^4) + q_i \right] \quad (16)$$

where $i = 1, 2, \dots, N$ represents the number of nodes and m the correspondent mass; therefore, N is also the number of differential equations involved in the problem.

This set of ODE has been integrated by means of Matlab's *ode45*, with initial conditions set to 0°C , whereas the number of nodes is set to 7: the six faces of the CubeSat, plus the wax-based engine.

Indeed, by considering black painting for the internal faces of the spacecraft and emissivity of $\epsilon = 0.6$ and an absorptivity $\alpha = 0.6$ for the coating of the paraffin wax cylinder unit, leading to a ratio $\alpha/\epsilon = 1$, the temperature of the wax unit settles to about 38°C and to about 42°C after 20 revolutions, in cold and hot cases respectively, with no huge differences to show (see Figure 16). Moreover, a simulation run considering a Sun synchronous orbit shows that - even in this hotter case - the coating is able to keep the wax under its melting temperature. Therefore, the chosen coating

Face	+x	-x	+y	-y	+z	-z
Hot case, °C	6.4	40.2	95.8	88.9	123.6	42.9
Cold case, °C	-28.6	-2.7	-2.5	-2.3	-0.7	0.2

Table 3 Spacecraft faces temperature in worst hot and cold cases

solution ensures that the temperature constraints are respected.

Such values of emissivity and absorptivity can be achieved by adopting a sandblasted metal surface finish, as mentioned earlier. For example, a Multi-Layer Insulation (MLI) can be selected and modelled in order to have an outer cover with those values of emissivity and absorptivity. An optimal choice could be a combination of internal layers enclosed in a Vapour Deposited Aluminum (VDA) cavity, optimally tuned in order to achieve the desired values of α and ϵ .

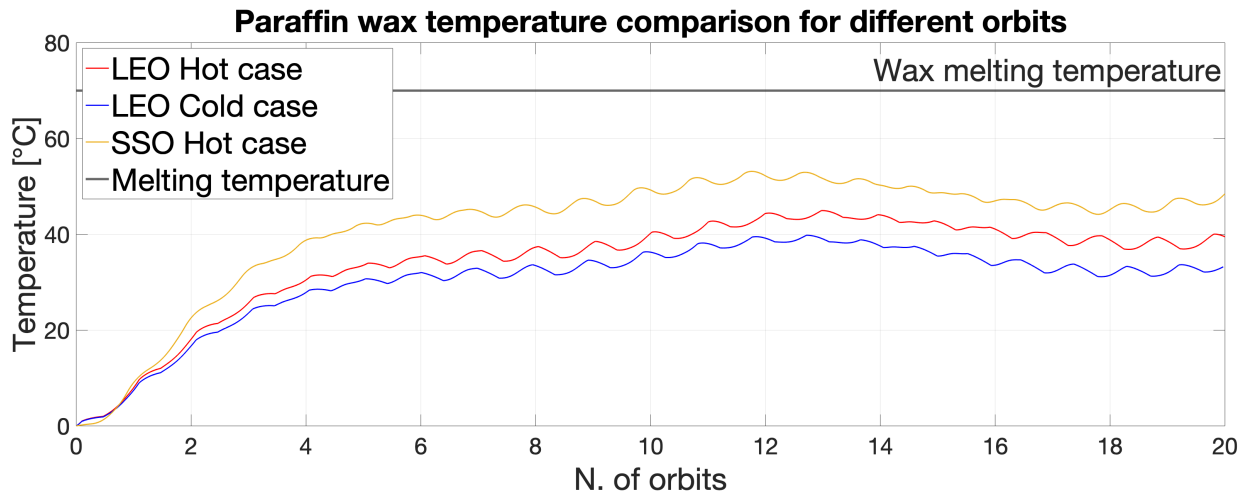


Fig. 16 Temperature evolution of the paraffin wax

As for the results, the differences between hot and cold cases are mainly related to the temperature of the faces of the spacecraft. Indeed, table 3 shows the differences in the computed temperatures among the 6 faces of the CubeSat. This analysis can be useful for later development and refinements in the configuration of the spacecraft itself (e.g. avoid a hot face for a component with lower temperature requirements, or vice versa).

This stem plot helps in giving a better picture of the temperature conditions in the worst cases:

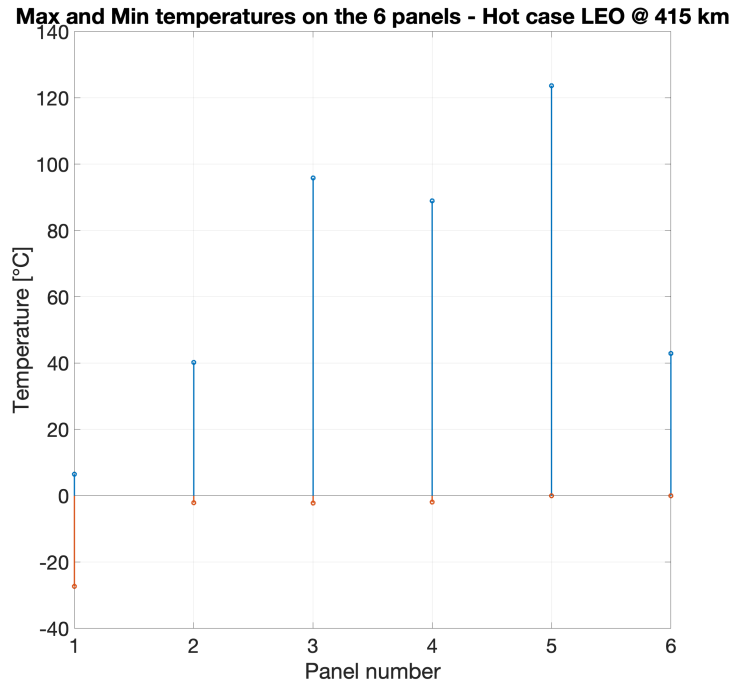


Fig. 17 Maximum and minimum temperature on the 6 faces of the spacecraft, hot case

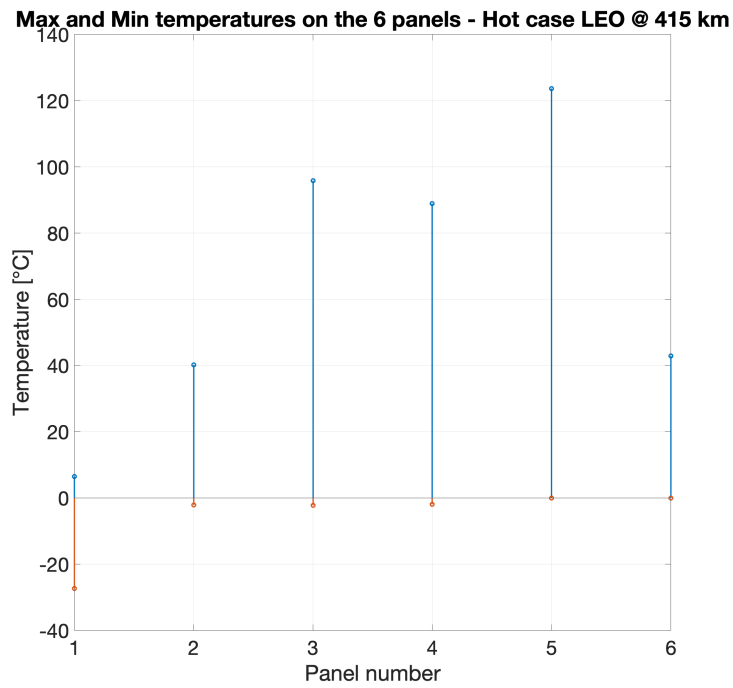


Fig. 18 Maximum and minimum temperature on the 6 faces of the spacecraft, cold case

VI. Deorbit Trajectory Design

The last part of this work involves the analysis of the performances related to the capabilities of a paraffin wax-based engine to deorbit a small satellite from a low Earth orbit.

As the design of the engine is not finalized yet, many assumptions were made and the results are inevitably affected; however, they still can be representative and perfectly suitable to give a hint on the real capabilities of the engine. Plus, some of the output results might serve as an input to the propulsion subsystem design, to have that work driven by the results coming from these simulations.

A. Mitigation strategies: natural decay vs chemical propulsion vs electrical propulsion

The main methods adopted nowadays for deorbiting a spacecraft can be divided into *natural decay*, *active systems* and *passive systems*.

In natural decay, after many orbital periods, the perigee height of the orbit decreases as a result of the interaction between the orbiting object and the effect of many forces (gravitational, mechanical, etc.). For bodies in low Earth orbits, however, the main effect is due to the atmospheric drag, the only dissipative force acting on the orbiting body. This aspect will be analyzed for the case study, for which it is exploited the fact that the altitude of the initial orbit (approximately 415 km) is low enough to allow an uncontrolled re-entry in less than 25 years after the end of life. The main parameters, when relying on natural decay, that influence the deorbit time are the initial altitude of the orbit (the higher it is, the less dense is the atmosphere, resulting in a longer deorbiting time) and the area-to-mass ratio of the spacecraft, as already mentioned previously, which at higher values correspond a reduced time for the spacecraft to enter into the atmosphere. Another effect that influences the deorbit time is the solar activity; indeed, a higher solar flux leads to a denser atmosphere in a particular region. Denser atmosphere, of course, reduces the re-entry time.

Natural decay is only viable if it is possible to prove that the 25 years limit will be respected, and the models for the re-entry prediction must be accurate enough to account for all of the aforementioned effects. When it is not possible to comply with such requirements, active methods should be used. Basically, they involve the use of a propulsive system capable of decreasing the orbit height by giving one or more impulses. This method classifies as *direct deorbit*, as it requires a single burn to inject the spacecraft into a Hohmann transfer orbit, characterised by the apogee coincident with the maneuver point, and a perigee low enough to allow this maneuver to happen with only one impulse. Indeed, usually the perigee is set to be lower than 120 km, so that the spacecraft is captured by the denser layers of the atmosphere, causing it to burn. Also, the absence of a second burn, reduces the amount of propellant mass required for this kind of maneuver; this is particularly good for spacecrafts with low mass, as in this case study. A negative aspect of using chemical propulsion for this purpose, is that - usually - a higher quantity of propellant mass is required, in order to account for this phase of the mission. However, this aspect concerns mainly more massive spacecraft orbiting at higher altitudes (e.g. 800 km), for which - in order to alleviate this problem - it may be considered a *partial deorbit* instead of a *full direct deorbit*, consisting in injecting the spacecraft not into a Hohmann transfer with perigee lower than 120 km, but instead of performing a maneuver that will lead the spacecraft to an orbit in the range of 200-400 km, and then just let it naturally decay; besides, the designer should always take into account that this natural decay must be such that - in any case - the spacecraft re-enters in less than 25 years. Moreover, as it will be shown in the results section, the deorbit with chemical propulsion ensures a much lower deorbit time with respect to the natural decay.

Another deorbit option is represented by *drag augmentation devices*, acting as a *passive method*: by enlarging the area-to-mass ratio of a spacecraft, more surface will be exposed and so more will be the resistance offered by air, especially at low altitudes. These strategies may involve the use of inflatable structures, such as *drag balloons* or non-inflatable structures, such as rigid booms, i.e. *drag sails*. The risks involved with these solutions is quite evident: the drag area needed to deorbit the spacecraft is pretty huge, and this increases the risks of collisions. That is why these solutions aren't easy to apply, especially for spacecrafts orbiting at altitudes higher than 500 km. Also, NASA Guideline [10] clearly states this kind of risk in section 6-1a of the same document.

VII. Graveyard orbit modelling and design

After the aforementioned literature review, in this final section will guide the reader through the details of the deorbit trajectory design. The mathematical modeling and the statement of the problem will blend in each subsection, as they walk side by side for each scenario considered (i.e. natural decay and powered re-entry).

In the end, the results will be presented as well as the conclusions, which will try to point out whether the wax-based engine is capable of not of deorbiting a spacecraft from an original height of 415 km.

A. Equations of motion

A detailed analysis, in order to assess the real capabilities of an engine, cannot assume impulsive maneuvers. Therefore, it is necessary to take into account and model the equations of motion of the spacecraft under the assumption of non-impulsive maneuvers, as the thrust acts over a significant time interval. So, the equations of the two-body problem cannot be anymore the ones presented previously, but must account for the thrust [11]; namely, they read:

$$\ddot{\mathbf{r}} = -\frac{\mu}{r^3}\mathbf{r} + \frac{\mathbf{F}}{m} \quad (17)$$

where \mathbf{F} is an external force acting on the spacecraft and m is its mass.

In this case study, the external force acting on the spacecraft is the thrust given by the wax-based engine, yielding:

$$\mathbf{F} = T \frac{\mathbf{v}}{v} \quad (18)$$

where T is the thrust and \mathbf{v} is the velocity vector. Note that the sign of this force is positive when the force acts in the direction of the velocity vector, in this case, since it is needed to lower the orbit, the impulse must be given in the opposite direction, therefore in the equations of motion used to model this problem the sign is, then, minus. Substituting eq. 18 into eq. 17 leads to:

$$\ddot{\mathbf{r}} = -\frac{\mu}{r^3}\mathbf{r} + T \frac{\mathbf{v}}{v} \quad (19)$$

where the Cartesian components are given by:

$$\begin{cases} \ddot{x} = -\mu \frac{x}{r^3} + \frac{T}{m} \frac{\dot{x}}{v} \\ \ddot{y} = -\mu \frac{y}{r^3} + \frac{T}{m} \frac{\dot{y}}{v} \\ \ddot{z} = -\mu \frac{z}{r^3} + \frac{T}{m} \frac{\dot{z}}{v} \end{cases} \quad (20)$$

As the engine is firing, the spacecraft mass decreases, because propellant combustion products are being discharged through the nozzle. The mass decrease rate can be computed as:

$$\frac{dm}{dt} = -\frac{T}{I_{sp}g_0} \quad (21)$$

where I_{sp} is the specific impulse and g_0 is the sea-level gravity acceleration.

As no analytical solution can be sought for such complex system of equations, both 23 and 21 must be rewritten as a system of linear differential equations in the form:

$$\dot{\mathbf{y}} = \mathbf{f}(t, \mathbf{y})$$

Where the state vector \mathbf{y} is, in this case, a 7x1 vector, made up by the position and velocity vectors, plus the mass. Therefore, we have [11]:

$$\mathbf{y} = \begin{pmatrix} x \\ y \\ z \\ \dot{x} \\ \dot{y} \\ \dot{z} \\ m \end{pmatrix}$$

its time derivative:

$$\dot{\mathbf{y}} = \begin{pmatrix} \dot{x} \\ \dot{y} \\ \dot{z} \\ \ddot{x} \\ \ddot{y} \\ \ddot{z} \\ \dot{m} \end{pmatrix}$$

and, finally:

$$\mathbf{f}(t, \mathbf{y}) = \begin{pmatrix} y(4) \\ y(5) \\ y(6) \\ -\mu \frac{y(1)}{r^3} + \frac{T}{m} \frac{y(4)}{v} \\ -\mu \frac{y(2)}{r^3} + \frac{T}{m} \frac{y(5)}{v} \\ -\mu \frac{y(3)}{r^3} + \frac{T}{m} \frac{y(6)}{v} \\ -\frac{T}{I_{sp} g_0} \end{pmatrix} \quad (22)$$

Of course, these equations only take into account the external force due to the thrust, in terms of acceleration. For deorbiting problems, especially at low altitudes, there are two other factors to consider: the gravitational perturbation and, of course, air drag. The final equation of motion is the following:

$$\ddot{\mathbf{r}} = -\frac{\mu}{r^3} \mathbf{r} + \mathbf{p}_{J2} + \mathbf{p}_{drag} + \frac{\mathbf{T}}{m} \quad (23)$$

Then, the thrust is considered to be acting constantly and only during the burning time; this can be simply integrated by using the following logic:

$$\mathbf{T} = \begin{cases} eq. 18 & \text{if } t < t_{burn} \\ 0 & \text{if } t > t_{burn} \end{cases} \quad (24)$$

B. Engine parameters

At the time being, it is very difficult to find any kind of work related to the design of a paraffin wax-based engine for CubeSats. Mainly, the works involving the design of hybrid engines is more focused on larger scales, such as rocket launchers. Indeed, no certain data about the engine parameters has been found and so, at this stage of the project, the design of the engine can't been finalised, only few indicative input data is given.

The main problem is related to the burning time: as [12] indicates, the works related to the design of hybrid engines - from various studies around the world - found clashing results on the burning time, ranging from 4.3 s up to a maximum of 80 s. But, again, these values are related to larger scale motors.

In this context, the burning time can be assumed to be derived by the following equation:

$$t_b = \frac{m_{prop}}{\dot{m}} \quad (25)$$

where m_{prop} is the propellant mass on-board the spacecraft, and \dot{m} is the propellant mass flow rate, given by:

$$\dot{m} = \frac{T}{I_{sp}g_0} \quad (26)$$

Given a hypothetical input value of thrust equal to 70 N, and a specific impulse of 320 s, it is straightforward to derive a burning time of approximately 44.8 s, which falls in the range of the values indicated in [12], and so it is a value that might be good for a first approximation. Moreover, from these data, it is also straightforward to derive - from Tsiolkovsky equation - the maximum theoretical deliverable ΔV , as:

$$\Delta V = I_{sp}g_0 \ln \left(\frac{m_0}{m_f} \right) = 330 \text{ m/s} \quad (27)$$

Summarising the input data used to set up the problem:

- Thrust = 70 N
- $I_{sp} = 320$ s
- Burning time = 44.8 s
- $\Delta V_{max} = 330$ m/s

As for the propellant mass, the scale of a 3U CubeSats sets some limitations in terms of maximum size and, incidentally, mass. As explained in the section related to the configuration of the spacecraft, the allowable space given to the engine is up to 1.5 U, therefore the grain will form accordingly to the already described geometry.

C. Ideal single impulse deorbit

An initial approach, to get a feeling of the order of magnitude of the results that should be expected, has been developed by following the algorithm described in [13], where the ΔV required to deorbit a spacecraft from a generic circular Earth orbit is derived by means of the following equation. It basically assumes that a Hohmann transfer can be performed between an initial circular orbit and a final one, whose perigee falls within Earth's thicker layers of the atmosphere; for an illustration of the problem, see figure 19.

$$\Delta V = V_{Ce} \sqrt{\frac{1}{\bar{r}}} \left[1 - \sqrt{\frac{2(\bar{r} - 1)}{\left(\frac{\bar{r}}{\cos\gamma_e}\right)^2 - 1}} \right] = V_{Ci} \sqrt{\frac{1}{\bar{r}}} \left[1 - \sqrt{\frac{2(\bar{r} - 1)}{\left(\frac{\bar{r}}{\cos\gamma_e}\right)^2 - 1}} \right] \quad (28)$$

where

- $\bar{r} = \frac{z_i + r_E}{z_e + r_E} = \frac{r_i}{r_e}$, orbit radius ratio
- $V_{Ce} = \sqrt{\frac{\mu}{r_e}}$, velocity of the circular orbit at the entry interface
- $V_{Ci} = \sqrt{\frac{\mu}{r_e}}$, velocity of the initial orbit
- γ_e , flight path angle at the entry interface
- z_i , altitude of the initial orbit
- z_e , altitude at the entry interface

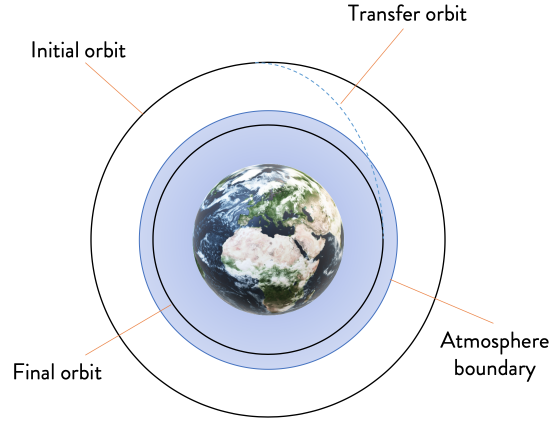


Fig. 19 Hohmann deorbit trajectory

- r_i , radius of the initial orbit
- r_e , radius at the entry interface
- r_E , Earth mean radius
- μ , Earth gravitational parameter

Then, to compute the true anomaly of the spacecraft at the entry interface, it is possible to use the following to equations:

$$\sin\theta_e = \frac{\tilde{r}}{e_d} \sqrt{\frac{a_d(1-e_d^2)}{\mu}} \quad (29)$$

$$\cos\theta_e = \frac{a_d(1-e_d^2)}{e_d r_e} - \frac{1}{e_d} \quad (30)$$

And extract the quadrant by using the inverse tangent operation:

$$\theta_e = \tan^{-1}(\sin\theta_e, \cos\theta_e) \quad (31)$$

where

- e_d , eccentricity of the deorbit trajectory
- a_d , semi-major axis of the deorbit trajectory
- $\tilde{r} = -\sqrt{\frac{\mu[2a_d r_e - r_e^2 - a_d^2(1-e_d^2)]}{a_d r_e^2}}$

The time of flight between the maneuver point (i.e. apogee of the deorbit trajectory) and the entry interface can be easily derived by means of the time law [11], yielding:

$$t(\theta_e) = \frac{\tau}{2\pi} \left[2 \tan^{-1} \left\{ \frac{1-e_d}{1+e_d} \tan \frac{\theta_e}{2} \right\} - \frac{e_d \sqrt{1-e_d^2} \sin\theta_e}{1+e_d \cos\theta_e} \right] \quad (32)$$

where

- $\tau = \frac{2\pi}{\sqrt{\mu}} a_d^{1.5}$, orbital period of the deorbit trajectory

Hence, the time of flight between the maneuver point - assuming that it happens at the perigee of the initial orbit - and the entry interface is given by:

$$\Delta t = t(\theta_e) - t(\pi) - t(\theta_e) - \frac{\tau}{2} \quad (33)$$

Then, the velocity at the entry interface can be computed:

$$V_e = \sqrt{\frac{2\mu}{r_e} - \frac{\mu}{a_d}} \quad (34)$$

D. Optimisation strategy

Though the previous approach still leads to reasonable results and is quite helpful to get a feeling for the results, it should be clear that it does not take into account some crucial effects that, instead, must be considered. Therefore, the previous algorithm represents the fitness function that has been used inside the optimization algorithm.

The optimization algorithm is based on the equations of motion described in the previous section, and so on equation 23. In this way, the physical effects related to a non-impulsive maneuver is considered, because the equations of motion - as already explained - take into account the fact that the engine fires through a finite amount of time. Moreover, aerodynamic drag, Earth's J_2 effect and propellant consumption are as well included in the model, and such equations of motion are numerically integrated by means of Matlab's *ode45*.

The objective function is set to be the scalar magnitude of the maneuver ΔV , while the constraints are imposed relatively to the flight path angle and the altitude at the entry interface. The control variables, instead, are represented by the true anomaly at the maneuver point, the ECI components of the maneuver ΔV and the time of flight. The initial guess for the ΔV is given by equation 28, i.e. the ideal approach described earlier.

This calls for a *Nonlinear Programming Problem* (NPL), where the trajectory optimization problem can be described by the following dynamic system:

$$\mathbf{z} = \begin{bmatrix} \mathbf{y}(t) \\ \mathbf{u}(t) \end{bmatrix}$$

where $\mathbf{y}(t)$ is the state variables vector and $\mathbf{u}(t)$ is the control variables vector. The state equations can be represented as follows:

$$\mathbf{y} = \frac{d\mathbf{y}}{dt} = f[\mathbf{y}(t), \mathbf{u}(t), \mathbf{p}, t] \quad (35)$$

Where \mathbf{p} is a vector of constant parameters, and the boundary conditions of the problem can be described by two dynamic variables, one defined for the initial time, t_0 , and one for the final time, t_f , with state and control variables evaluated at these times.

Therefore, the aim is to minimise the scalar objective function:

$$J = \phi[\mathbf{y}(t_0), t_0, \mathbf{y}(t_f), t_f, \mathbf{p}] \mapsto \min$$

In this way, the script numerically integrates eq. 23, while computing the errors in the target constraints, trying to drive them to zero. The two errors are computed by considering the difference between the computed value and the target one, with respect to the altitude and the flight path angle at the entry interface:

$$\epsilon_z = z - z_t$$

$$\epsilon_\gamma = \gamma - \gamma_t$$

Of course, the algorithm also requires upper and lower boundaries on the control variables. For such purpose, they have been chosen as:

- $180^\circ \pm 10^\circ$, for the true anomaly at the maneuver point, and also for the other control variables, symmetric conditions are chosen. In this case, the maneuver point should fall around the perigee of the initial orbit, which will turn into the apogee of the transfer orbit

- $\Delta V_{guess} \pm 15\%$, i.e. the lower and upper bounds are set to be between $\pm 15\%$ of the guess value of ΔV
- $TOF_{guess} \pm 30s$, for the time of flight between the maneuver point and the entry interface.

The optimization algorithm used is based on Matlab's *fmincon* and *gamultiobj*. The followed strategy was to give, as input to the genetic algorithm, the guess values computed with eqs. 28 - 33, using *gamultiobj* to sweep the solution space and then refine the results with *fmincon*.

VIII. Results

In this final section, the results of the trajectory optimization problem will be presented. The two scenarios compared are related to the natural decay of the orbit and to the powered re-entry. The comparison is mainly driven by the fact that the spacecraft will rely only on this engine, and so it can be seen as a single-point failure; therefore, in the case of such unfortunate event, it will be shown that - however - also with a natural decay of the orbit, the international guidelines will be respected.

Before going into the details of the results, let us state the initial conditions that are common to both powered and non-powered re-entry trajectory. As already said, the initial orbit is a constraint of the mission, because it is imposed by the deployment mechanism attached to the ISS. Therefore, the initial orbital elements are given by:

Orbital element	Value
Semi-major axis, km	6793
Eccentricity	0.0011
Inclination, deg	51.6
Right ascension of the ascending node, deg	0 (or user defined)
Argument of perigee, deg	0 (or user defined)
True anomaly, deg	0 (or user defined)

Table 4 Initial orbital elements

The orbit in the ECI frame is represented in Figure 20, while its ground track after one cycle and one day is shown in figures 21 and 22 respectively.

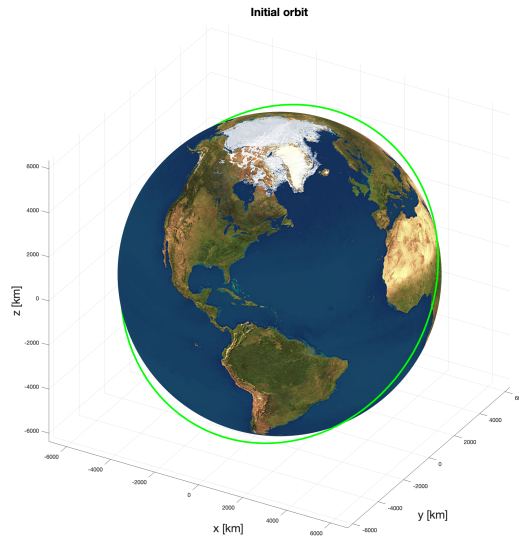


Fig. 20 Plot of the initial orbit

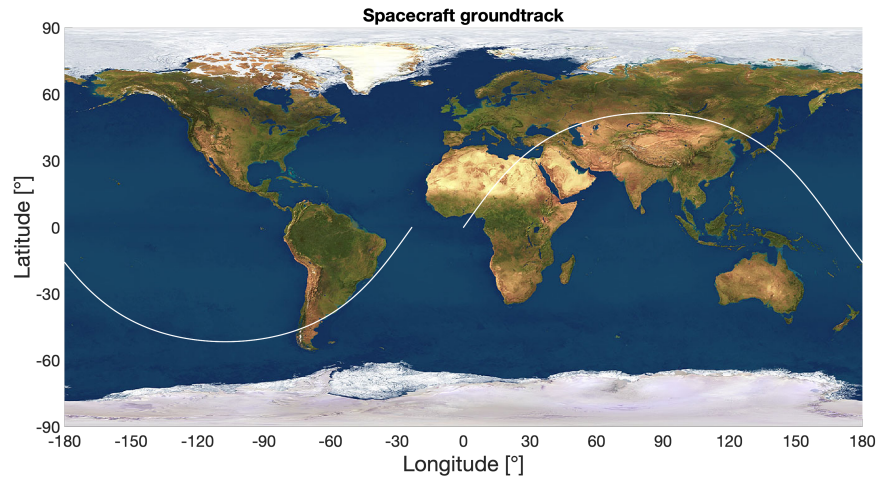


Fig. 21 Spacecraft ground track after 1 orbit

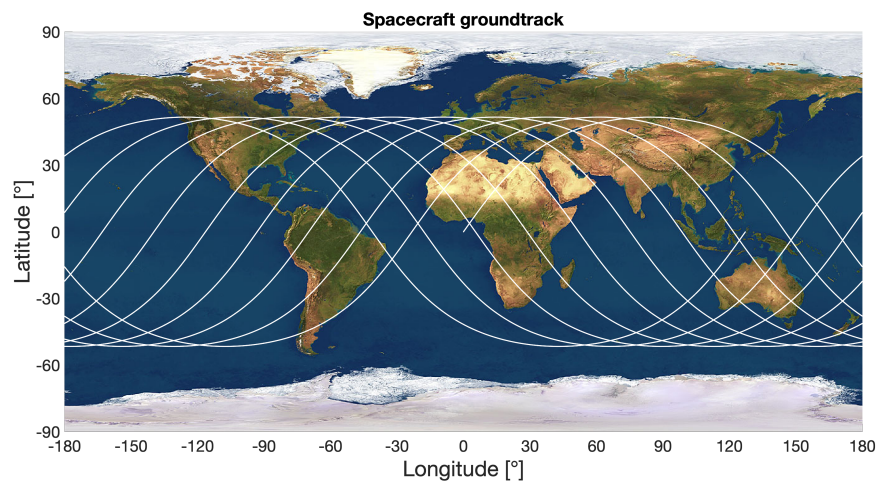


Fig. 22 Spacecraft ground track over 1 day

A. Natural decay

In this case, only air drag is considered to act on the spacecraft. From Figure 23 it can be seen that the orbit decays in less than 4 years.

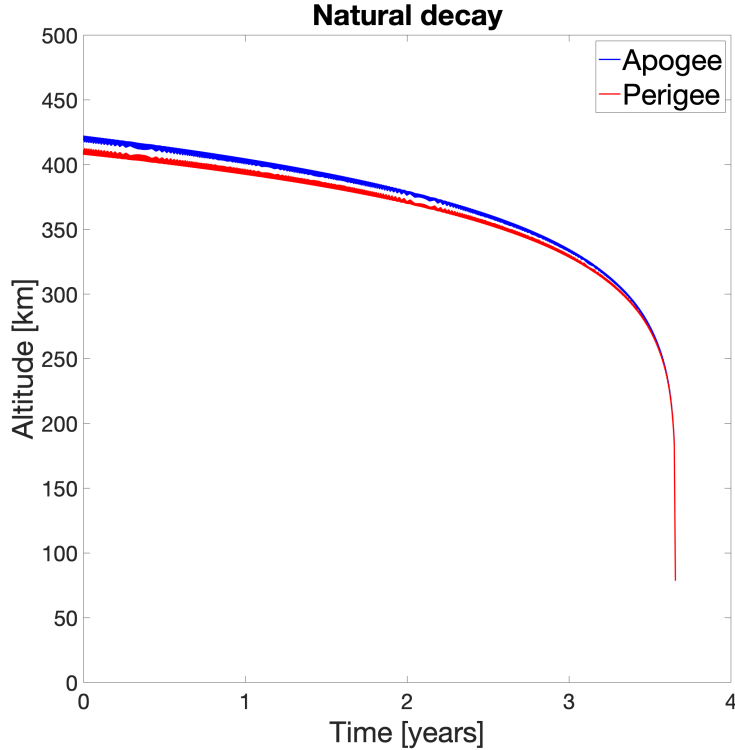


Fig. 23 Altitude of the spacecraft for uncontrolled re-entry

This kind of result falls within the expectations, as the spacecraft already lies in a very low orbit and is characterised by a mass of less than 5 kg. Hence, even in the case of a failure of the engine, the spacecraft re-entry time still complies with the 25 years limitation imposed by the international guidelines.

B. Powered re-entry

In the case of powered re-entry, the input parameters used for the engine are the ones described in section VII.B, while - as for the control variables, the target flight path angle is set to -2° and the target altitude is set to 78 km, as it is assumed to be an optimal altitude for which a spacecraft burns into the atmosphere. The results for the ΔV optimization are summarised in table 5.

Method	ΔV , m/s	Time of flight, min
Guess value	144.19534	28.049
Genetic algorithm	185.87871	28.030
fmincon	182.39246	28.130

Table 5 Results, in terms of ΔV and TOF of the optimization

Note how the guess value of the ΔV is quite lower with respect to the results of the optimization process; this is exactly a reflection of what discussed earlier in terms of the approximations used for the computation of the ideal ΔV : the guess procedure does not take into account the full equations of motion of the spacecraft with all the disturbances, the optimization algorithm does. However, the results in terms of time of flight are quite similar and are way below the international guidelines threshold.

In Figure 24 the reader can find the plot of the optimised deorbit trajectory, where there is the detail of the arc interested by the firing of the engine, which lasts for 44.8 s, i.e. approximately 0.00124° in terms of angular sweep. This

maneuver requires less than 1 kg of propellant.

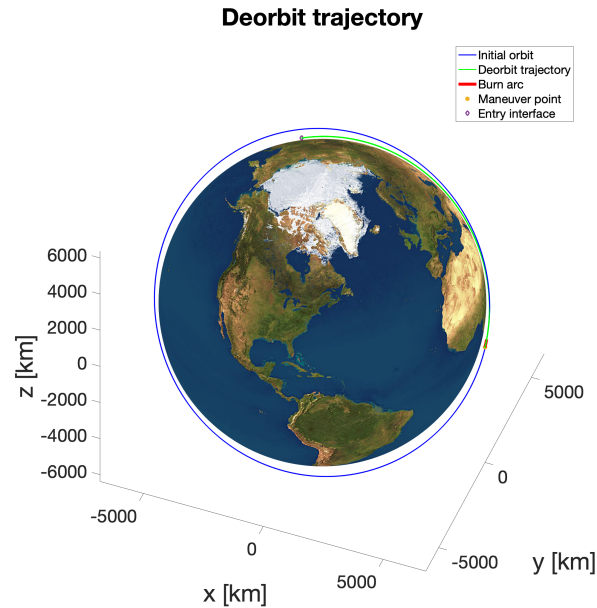


Fig. 24 Optimal deorbit trajectory with target entry interface of 78 km

C. Possible constraints on the propulsion subsystem design

As indicated in Section VII.B, the theoretical maximum ΔV is in the order of 330 m/s, and so it should be able to deorbit the spacecraft with one impulse. However, as the design of the engine isn't ready yet, it is possible to use these results as an input to the propulsion subsystem for the later stages of the design. For example, a driver to the design of the engine can be related to the burning time: with the burning time derived by considering the ratio between propellant mass flow rate and propellant mass computed according to the optimised trajectory, this kind of maneuver is perfectly achievable and allows the re-enter of the spacecraft in about 30 minutes. But this should not be an issue; indeed, other simulations (see Table 6) with reduced burning time show a decrease in the needed ΔV to complete the maneuver, while leaving almost unchanged the time of flight between the maneuver point and the entry interface.

Method	ΔV , m/s	Time of flight, min
Guess value	144.19534	28.049
Genetic algorithm	160.99768	28.045
fmincon	79.55733	28.132

Table 6 ΔV optimisation with $t_{burn} = 10$ s

IX. Conclusions

Despite the initial orbital conditions have been constrained by the assumptions of being released by the ISS, the developed tool is able to simulate any kind of Earth orbit and any kind of spacecraft, because each block that makes up the tool was built following a parametric approach. Therefore, the developed mission profiles implementation may be organised as needed, for future mission development.

This work gave also a first answer to the research objective, i.e. if it is possible to use a paraffin wax-based engine in order to deorbit a small satellite. It has been shown that it works and the re-entry times are absolutely reasonable

and compliant with the international regulations. However, still no satellites have implemented this kind of propulsion system, and so this is just a feasibility analysis based on few assumptions on the real capabilities of the engine. For this reason, a lot of simplifying assumptions have been made, which strongly limited the work. However, the obtained results are still valid to prove that it is feasible to use a wax-based engine and, moreover, to cast it directly in microgravity.

This work, however, can't be representative of the full feasibility of the mission. Instead, it can be used as a basis to develop and refine all mission aspects covered throughout the thesis, and - moreover - to implement new analysis and subsystems design. The latter is of the utmost importance, as a refined design of the propulsion subsystem will help in defining the requirements for the other subsystems, such as the power generation, active thermal control for melting the wax, a thermal bus design - which is crucial for conveying the wax inside the combustion chamber. After defining all of these aspects, a more representative configuration can be characterised, and this will come in handy for a FE analysis on a commercial software, such as ESATAN or similar.

References

- [1] Choi, M. K., "Phase Change Material for Maintaining Temperature Stability of IceCube Type of CubeSats in LEO," *13th International Energy Conversion Engineering Conference*, 2015, p. 3984.
- [2] *Candlewax Rockets: A green alternative for in-space propulsion*, ??? URL <https://www.media.mit.edu/projects/candlewax-rockets-a-green-propellant-alternative/overview/>.
- [3] *COMPASS ERC*, ??? URL <https://www.compass.polimi.it>.
- [4] Stober, K. J., Wanyiri, J., Sanchez, A., Hooper, M., Mazumder, M., Jiwani, S., Waft, C., Joseph, C., Lifson, M., and Wood, D., "An Investigation of the Centrifugal Casting of Paraffin Wax on Earth and in Microgravity," *AIAA Propulsion and Energy 2019 Forum*, 2019, p. 4012.
- [5] Gilmore, D. G., and Donabedian, M., *Spacecraft thermal control handbook: cryogenics*, Vol. 2, AIAA, 2003.
- [6] *National Oceanic and Atmospheric Administration (NOAA)*, ??? URL <https://www.ncdc.noaa.gov/>.
- [7] Garzón, A., and Villanueva, Y. A., "Thermal analysis of satellite libertad 2: A guide to Cubesat temperature prediction," *Journal of Aerospace Technology and Management*, Vol. 10, 2018.
- [8] Wertz, J. R., *Spacecraft attitude determination and control*, Vol. 73, Springer Science & Business Media, 2012.
- [9] SPACE, A., "Solar Power GmbH 0.32 Quad Junction GaAs Solar Cells datasheet," 2019.
- [10] Standard, N. S., "Guidelines and assessment procedures for limiting orbital debris," *NASA NSS*, Vol. 1740, 1995, p. 14.
- [11] Curtis, H. D., *Orbital mechanics for engineering students*, Butterworth-Heinemann, 2013.
- [12] Leccese, G., Cavallini, E., and Pizzarelli, M., "State of Art and Current Challenges of the Paraffin-Based Hybrid Rocket Technology," *AIAA Propulsion and Energy 2019 Forum*, 2019, p. 4010.
- [13] Milstead, A., "TECHNICAL NOTES Deboost from Circular Orbits," *Journal of the Astronautical Sciences*, Vol. 13, 1966, p. 170.